The Assembly of Coated Nanocrystals†

Luis M. Liz-Marzán*,‡ and Paul Mulvaney*,§

Departamento de Química Física, Universidade de Vigo, 36200, Vigo, Spain, and Chemistry School, University of Melbourne, Parkville, VIC, 3010, Australia

Received: December 27, 2002

The formation of nanostructured materials through the assembly of nanocrystals is described, focusing in particular on silica and other metal oxide coated core particles. The preparation and optical characterization of core−shell materials are reviewed, and some of the unique properties of core−shell materials are presented. Shell layers are shown to serve various functions. They may increase colloid stability, aid dispersion in various media, alter the optical and electrical properties of the core, add robustness, or provide a contiguous framework from which inverse lattices may be generated. The assembly of the particles into well-defined thin films and two-dimensional and three-dimensional crystals is discussed, and the resultant optical properties are reviewed. Approaches to increase the topological complexity are studied, and the potential for the creation of a variety of space-filling nanostructures (such as inverse lattices, opals, and photonic crystals) is illustrated.

1. Introduction

Classically, a sample of any bulk material exhibits two obvious length scales: the first is simply its macroscopic size, and the second, less-obvious one is a nanometer periodicity that is due to the lattice structure of the component atoms or other underlying constituents. Consequently, materials are usually characterized at both a macroscopic level and a nanoscopic level. For example, bulk crystals may diffract visible, IR, or microwave radiation, depending on their macroscopic dimensions. Conversely, at the atomic or molecular level, X-ray diffraction occurs. Similarly, there are atomic or molecular lattice vibrations, as well as collective acoustic and optical phonon modes of the entire ensemble. One can excite single electrons or collective plasmon modes. The electrons give rise both to high-frequency conductivity and to a bulk DC conductivity. There are unpaired electrons, resulting in magnetic moments, and there are bulk magnetic effects from the coupling of the individual electron spins. In all these cases, bulk properties arise from collective or coupled atomic effects and usually operate at a slower time scale, lower energy level. Usually, these atomic and bulk properties do not correlate in any simple fashion. For example, from the C−C stretching frequency of carbon atoms, one may estimate an atomic bond stiffness of $\sim 6 \times 10^2$ N/m. On the basis of this observation, one would expect that a small, centimeter-sized piece of polyethylene would be quite stiff, similar to wood. Yet, bulk polyethylene is a very flimsy material. Individual chemical bonds are generally much stronger than the resultant normal, lateral, or torsional stiffness of the bulk material, irrespective of the presence of defects and impurities. The strength and properties of the bulk material are determined by larger-length-scale mechanical and chemical interactions, rather than by the constituent molecular bonding. Novel macroscopic materials will ensue when all materials can be constructed on length scales other than purely atomic or molecular scales.

This dichotomy into molecular properties and macroscopic, collective properties is a strong impediment to materials scientists. Ideally, one should be free to construct materials on a variety of length scales. In Table 1, we have listed some well-known forces and properties of spheres, which are strongly dependent on size. The key concept, which we explore in this review, is the extent to which we can introduce tunability into the material properties by constructing macroscopic materials from nanocrystal-based components, rather than from atoms or molecules. The two basic parameters with which we are concerned are the size of the nanocrystal, which determines the magnitude of the relevant properties of the building block, and the spacing between the nanocrystals, which controls the coupling of properties across the material. Later in the review, we consider how different geometries or topologies can also be utilized to create new lattice structures.

To demonstrate how this idea works, consider a metal film. The conductivity of the film may be estimated using the relation

$$\sigma \approx Ne^2 R_{\mathrm{bulk}}/m v_{\mathrm{F}} \tag{1}$$

Here, v_{F} is the velocity of the conduction electrons at the Fermi energy, N the concentration of conduction electrons, and R_{bulk} the scattering length between collisions of the electrons with the lattice or defects. Classically, electrons lose their energy at a frequency or rate ω_{d}, which is given by the equation

$$\omega_{\mathrm{d}} = v_{\mathrm{F}}/R_{\mathrm{bulk}} \tag{2}$$

The conductivity of a normal metal is high and *decreases* as the temperature increases, because of phonon interactions, which decrease the mean free path. However, it has long been known that, in materials with high grain resistance or a high level of dislocations, an activation-controlled conductivity is observed.

$$\sigma \approx \sigma_0 \exp(-E_{\mathrm{a}}/k_{\mathrm{B}}T) \tag{3}$$

† Part of the special issue "Arnim Henglein Festschrift".

* Authors to whom correspondence should be addressed. E-mail: lmarzan@uvigo.es, mulvaney@unimelb.edu.au.

‡ Universidade de Vigo.

§ University of Melbourne.

10.1021/jp027835b CCC: $25.00
Published on Web 06/27/2003

TABLE 1: Some Size-Dependent Material Properties and Interaction Forces for Spheres

property	size dependence
capacitance	$1/(4\pi\epsilon_0 a)$
vibration frequency[a]	$\omega^2 = k/m$
viscosity[b]	$\eta = 1 + 2.5\phi + [6.25 + (2.1/\tau_B)]\phi^2 + ...$
electrostatic energy[c]	$U_{elec} = 2\pi\epsilon_r\epsilon_0 a\psi_0^2 \ln(1 + \exp(-\kappa D))$
van der Waals energy[d]	$U_{vdw} = -aA_H/(12D)$, for $D \ll a$
magnetic coupling[e]	$U_{mag} = -m^2(3\cos^2\theta_{i,j} - 1)/(4\pi\mu_0 r_{i,j})$
diffusion coefficient[f]	$D = k_B T/(6\pi a\eta)$
bulk mechanical properties[g]	
normal stiffness	$k = Et^3w/(4L^3)$
eigenfrequency	$f = 0.162(t/L^2)(E/\rho)^{1/2}$
diffraction wavevector	$2\pi/a$
breathing frequency[h]	$\omega = \tau\alpha/a$
Laplace pressure[i]	$P = 2\gamma/a$
metal conductivity[j]	$G = Ne^2a/mv_F$

[a] This equation is used in reverse. From the IR vibration frequency, the stiffness of chemical bonds may be estimated; here, m is the reduced mass of the atoms constituting the bond. [b] For the case of hard spheres with zero adhesion in a Newtonian fluid, the viscosity η increases directly with the particle volume fraction ϕ, which varies with the cube of the particle radius: $\phi = (\text{particles})4\pi a^3/3$. [c] The coulombic interaction energy between spheres separated by a distance D in an electrolytic solvent is dependent on the dielectric constant of the medium (ϵ_r), the surface potential relative to the bulk solvent (ψ_0), and the inverse Debye length (κ). [d] The van der Waals interaction energy U_{vdw} is a function of the surface separation and scales directly with the Hamaker constant A_H, which is a complex, frequency-dependent function of the polarizabilities of the interacting spheres. [e] The magnetic dipole of a magnetically polarizable medium is given as $m = 4\pi a^3\mu_0\chi H/3$, where χ is the magnetic susceptibility, H the magnetic field, and μ_0 the permeability of free space. The interaction energy is dependent on the relative angle and separation between each pair of particles i,j. The moments themselves are induced by the applied field and, hence, are assumed to be aligned in the same direction as H. [f] The diffusion coefficient either may be a short-term quantity, which measures the local diffusivity of the sphere in the solvent, or is a longer-term quantity averaged over motion through the solution and includes numerous interactions with other spheres. [g] For completion, we note that a simple beam has a stiffness due to a point force applied at the end; the stiffness is dependent on the thickness t, width w, length L, and Young's modulus E. The fundamental frequency of such a beam also is dependent on the beam density. The construction of composite nanocrystal assemblies from nanocrystals allows the values of E and ρ to be tuned over large ranges and, hence, permits the material properties to be tailored. [h] Here, $\tau \cot \tau = 1 - \tau^2/(4\kappa^2)$, α is the longitudinal speed of sound in the material, β is the transverse speed, and κ is the ratio of β/α. [i] γ is the surface tension. [j] N is the conduction electron concentration, m the electron mass, and v_F the Fermi velocity. This equation holds for sizes below the bulk mean free path, which, for good conducting metals, is 30−55 nm.

The activation energy is attributed to tunneling across the grain boundary or dislocation. Through the assembly of metal nanocrystals, macroscopic metals whose conductivity can be controlled through the creation of well-defined barriers between the particles can be created.[3,4] Müller and colleagues recently quantified the bulk conductivity of a coated nanocrystal assembly, in terms of the individual particle sizes, the parallel conduction routes, and the barrier thickness.[5] For extremely small gold nanocrystals, the coulombic charging energy must be included, because of the small electrical capacitance of the component particles (see Table 1). Although the absolute conductivity may be lower than that for a pure metal, it becomes tunable over orders of magnitude by the incorporation of nanometer-scale coatings. The salient point here is the ability to modulate the bulk properties through the incorporation of new length scales into the material. In this case, the conductivity is controlled by the barrier thickness (coating thickness) and the number of barriers per unit length (particle size).

Perhaps a more general case of using length scale to control material properties is that of polymers. Chemists have long manipulated polymer chain length to vary the properties of the resultant bulk material. Tensile strength, ductility, color (in conjugated polymers), viscosity, and elasticity can all be varied through orders of magnitude through the fact that the component polymer chains can be synthesized with molecular weights in the range of 10^2-10^7 daltons.[6] Branching similarly enables structural variations in three dimensions to be introduced.

Gradually, a similar transition is overtaking conventional inorganic materials science. This shift can probably be traced back to the breakthroughs in zeolite synthesis in the early 1980s, which revolutionized the basic links between geometry and catalysis in lattices. The creation of three-dimensional (3D) networks of cavities and tunnels in zeolites with sizes above the atomic scale made possible materials in which time-dependent processes such as diffusion could be controlled. If the "molecular" components of a solid can be altered in size, then materials with tailored responses to energy and mechanical stresses can be envisaged. What is needed to achieve this is the inorganic equivalent of the polymer chain. These are, of course, colloid particles. The creation of materials from building blocks larger than the atomic scale will lead to a merging of top-down and bottom-up approaches to materials science. Materials are needed with Bragg spacings that span from X-ray wavelengths to those of radio waves. Materials are needed with mechanical relaxation times that span a range from picoseconds to years. Materials are needed that can conduct single electrons over macroscopic distances or trap single photons within cavities. Unfortunately, in contrast to the mature field of polymeric materials, the study of nanocrystal-based materials is comparatively new. Some twenty years have been required for the syntheses of nanoscale metals, semiconductors, magnetic and ceramic materials to attain the necessary monodispersity and reproducibility for length-scale control to be truly viable.[7−10] For reasons of brevity, we focus here on the use of core−shell structures as just one route toward spatial and topological control of material architecture. We recognize that there are many means to create nanostructured materials with properties similar to those reviewed here. Similarly, although many different combinations of materials have been chosen for the synthesis of particles with core@shell geometry,[11] we restrict ourselves here to two basic categories: *nanocrystals coated with silica*, and *metal nanoparticles coated with semiconducting oxides*. With these two categories, we exemplify the use of inert coatings to create nanostructured materials with tunable length scales, as well as the combination of elements with different electronic structures to achieve materials with novel properties.

The long-term motivation for this work is a better understanding of the relationships between material topology and material function. Increasing the topological complexity of nanocrystal-based structures allows for the creation of designer materials. A basic map of some of the topological colloid-based objects that are being devised, designed, and synthesized is shown in Scheme 1. By no means is this scheme comprehensive; it illustrates the four basic concepts for particle modification, which are size control, shape manipulation, layered structures, and nanocrystal ordering. Combinations of these four processes can be readily envisaged. Three of these four pathways from single nanocrystals to more complex materials are well understood mechanistically. Size control is determined by nucleation and growth kinetics and the efficacy of capping agents in preventing Ostwald ripening and coalescence. Colloid structuring is largely controlled through manipulation of colloid and

SCHEME 1. Basic Aspects of Nanocrystal Topology.

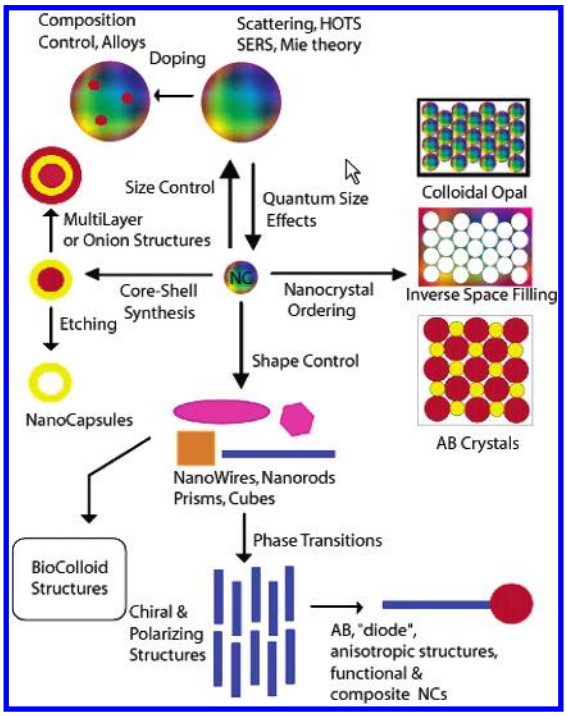

surface forces such as double layer repulsion, capillary forces, sedimentation, and electrophoresis or magnetophoresis. Finally, layered colloids can be synthesized when there is sufficient control over deposition and nucleation within a nanocrystal system. Shape control is the exception. Shape control is the inorganic equivalent to branching in polymers and is poorly understood. Mechanisms for imposing shape change are only now emerging and seem to rely on the vagaries of surfactant adsorption to specific crystal facets in most successful cases. This review attempts to address only materials that involve some form of coating, or coating plus assembly.

2. Coated Nanocrystals

We begin by summarizing some of the key synthetic improvements and breakthroughs in the creation of different core−shell nanocrystals. We present a survey of several procedures that have allowed the encapsulation of metal, semiconductor, and magnetic nanocrystals with metal oxides, as well as the main advantages that have thereby been acquired.

2.1. Coating of Nanocrystals with Silica. The use of silica as a coating material has a long tradition in colloid science. One of the major reasons is the anomalously high stability of silica colloids, especially in aqueous media, but other reasons include easy control of the deposition process (and the shell thickness), its processability, chemical inertness, controllable porosity and optical transparency. All these properties make silica an ideal, low-cost material to tailor surface properties, while basically maintaining the physical integrity of the underlying core nanocrystals.

One of the great advantages of a core−shell geometry for colloid particles is that the stability of the colloid will be determined by the nature of the shell material. The only effect that the core exerts upon two approaching spheres is through van der Waals attraction. These forces decay as $1/r^6$ (Table 1); therefore, they are important only for very thin shells. Contrary to Derjaguin−Landau−Verwey−Overbeek (DLVO) theory,[12] silica sols in the size range of 10−100 nm have been observed to possess a remarkable stability at very high salt concentrations (e.g., 0.15 M NaCl) at pH ≥10.5,[13,14] and even at their isoelectric point (pH_{iep}).[15] The main factors favoring the remarkable stability of silica sols are that (i) the Hamaker constant (A_H) of silica is much lower than those of metals, latex, and other oxide particles, and, (ii) at the silica−water interface at pH ≥10.5, a polymeric silicate layer is present on which highly hydrated cations are very tightly bound.[16] The silicate layer confers steric and electrostatic protection on the silica particles in the pH range above pH_{iep} and below pH 10.5, whereas, at pH_{iep}, only the steric barrier is present. These special properties are the reason why soluble silicates, usually sodium silicates, are universal dispersants of many electrostatic colloids.[17] Well-hydrated silica[15] and other colloids that have been exposed to aqueous silicate[18] acquire high adsorption densities of aqueous silica or silicates. In contrast, at pH ≥11 and 0.15 M NaCl, the same silica sols are observed to undergo coagulation, as predicted theoretically. This is because the steric silicate coating is no longer present on the surface of the silica sol, as the majority of large polymeric silicates are dissolved by OH^- ions to form smaller units.[19] Iler[15] and, more recently, Furlong et al.[18] detected the desorption (or lack of adsorption) of oligomeric and polymeric aqueous silica at pH values >10.5.

Even though the core properties of silica-coated nanoparticles are unaffected, should they become coagulated, for many purposes such as the formation of two-dimensional (2D) and 3D crystals, it is still desirable for them to remain dispersed. Such dispersibility can be achieved using silica as an encapsulating shell. Thus, silica coating has been employed for over half a century[20] for the enhancement of the colloidal stability of different particles. However, only recently has it been possible to adapt these procedures to the coating of nanocrystals,[21,22] which is complicated, because of their extremely high curvature.

Ohmori and Matijevic[23] made use of the classical Stöber method[24] (base-catalyzed hydrolysis and condensation of tetraethoxysilane (TEOS)) to coat hematite (Fe_2O_3) spindles in ethanol. Later work by Philipse et al. employed a combination of silicate condensation and the Stöber method for coating magnetite (Fe_3O_4) superparamagnetic nanoparticles[21] and boehmite (AlOOH) nanorods.[22] Following Philipse's work, the silica coating of magnetite was later modified by other groups.[25−27] The ability to control magnetic interactions is an important consequence of the coating of magnetic particles, which has been explored by Donselaar et al. for particles in solution,[28] and by Aliev et al. in close-packed thin films.[29]

The silica coating of metal colloids has also been studied in detail, especially during the past decade. This type of core−shell particle presents an additional difficulty: the chemical mismatch between the core and the shell materials. Several routes have been pursued. Ohmori and Matijevic[30] prepared $Fe@SiO_2$ by an indirect path that was comprised of the initial coating of hematite spindles,[23] followed by reduction of the core within a furnace at 450 °C while passing a stream of H_2 gas. The high temperature promoted the sealing of the pores of the silica shell, thus avoiding further oxidation of the metallic core. Liz-Marzán and Philipse[31] were the first to synthesize $Au@SiO_2$ particles in solution successfully, through the formation of nanosized gold particles on the surface of small silica spheres by heterocoagulation, followed by dilution with ethanol. Secondary growth was achieved by means of the Stöber method,[24] so that gold was embedded as a core. Although this process led to a mixture of labeled and unlabeled silica particles, these colloids could be applied to the study of the dynamics of concentrated silica colloids, using an index-matching technique.

A method that has provided substantially better results was later designed by Liz-Marzán et al.[32,33] The method was based

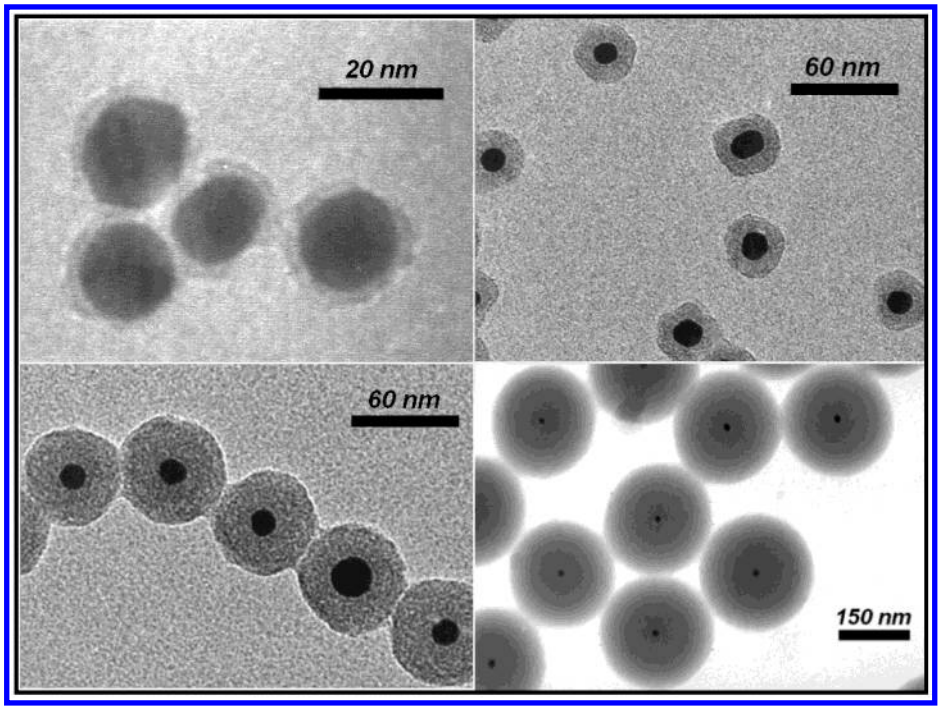

Figure 1. Examples of gold nanoparticles (15 nm in diameter) coated with silica shells of various thickness.

on the use of silane coupling agents[34] as surface primers to provide the gold nanoparticle surface with silanol groups, thus rendering it compatible with silicate moieties. After the surface had been modified, a slow deposition of a thin silica shell was effected from a sodium silicate solution. The shells could then be grown by transfer into ethanol and careful addition of ammonia and TEOS, resulting in monodisperse colloids, as shown in Figure 1. This system proved to be ideal for a systematic study of the optical properties of core−shell particles.[33,35] The same method was later extended to Ag@SiO_2,[36] although new difficulties arose, because of the dissolution of the silver cores when concentrated ammonia was added to increase the thickness of the silica shell. Subsequent studies[37,38] examined the possibility of chemical reactions taking place within the cores, because of the porosity of the shells.

Because of the slow rate of silica deposition in water, this method allows one to preserve the shape of the original core in the initial stages of coating. Chang et al.[39] exploited this fact by coating gold rods with silica. Similar results were reported by Obare et al. for chemically synthesized nanorods.[40]

Hall et al.[41] used the same method to incorporate chemical functionality in the shell, by means of the copolymerization of silane coupling agents with TEOS during the final growth step. Hardikar and Matijevic[42] later demonstrated that, for larger silver particles (60 ± 5 nm) stabilized with a complex surfactant (Daxad 19), no coupling agent is necessary for silica coating through TEOS hydrolysis in 2-propanol. Similarly, Xia and co-workers coated poly(vinyl pyrrolidone) (PVP)-stabilized silver nanorods with silica without the use of a coupling agent.[43] Again, the problem of silica dissolution by ammonia was reported by these authors, so that coated particles (rather than hollow silica shells) could only be obtained if they were separated from the ammonia by centrifugation some 20 min after addition of the base. The same group reported that the procedure works for commercial gold nanoparticles, although the nature of the surface coating on these particles was not specified.[44] Mine et al. also recently found[45] that standard, citrate-stabilized gold nanoparticles can be homogeneously coated with relatively thick shells without the use of a silane coupling agent, through careful tailoring of the concentrations of ammonia and TEOS, and through the proper addition sequence.

The possibility of using silica-coated gold for electronic devices was demonstrated by Yau et al.,[46] who studied single electron tunneling through the silica shell of Au@SiO_2 with scanning tunneling microscopy (STM) and observed Coulomb staircases for both anodic and cathodic potentials. Makarova et al.[47] attempted to measure the hindered diffusion of tracer molecules within nanosphere cavities. They trapped fluorescent dye probes inside silica shells by adsorbing the dye onto the surface of gold cores prior to silica coating and then dissolving off the cores, leaving the dye molecules locked inside the SiO_2 shell. They observed significant differences in the fluorescence of the dye molecules, depending on whether it was in bulk solution, trapped on the gold cores in Au@SiO_2, or trapped inside the hollow SiO_2 nanospheres. A further advance by the same group was the use of surfactants to create mesoporous silica shells on gold nanoparticles coated with a thin silica layer.[48] Ostafin and co-workers explicitly mentioned the need for an initial standard coating to stabilize the metal colloids during the growth of the mesoporous shell.

Other methods have been designed for the preparation of Ag@SiO_2. Adair and co-workers[49] reported the formation of silver nanocrystals within the droplets of water-in-oil (W/O) microemulsions, followed by silica coating through the polymerization of TEOS within the same droplets. A similar method was used by Martino et al.[50] to prepare silica gels that were loaded with gold nanoparticles. Pastoriza-Santos and Liz-Marzán prepared Ag@SiO_2 particles through reduction of the Ag^+ cation by *N*,*N*-dimethylformamide (DMF)[51] and DMF/ethanol mixtures,[52] in the presence of 3-aminopropyltrimethoxysilane (APS). High temperatures were needed to achieve fast reduction of the silver salt, prior to condensation of the organo-silica shell.

A different approach was followed by Schmidt and co-workers, who used various organosilanes as building blocks and spacers to introduce functionalities within the nanoparticle structure, which could then be subsequently employed for the preparation of more complex materials.[53]

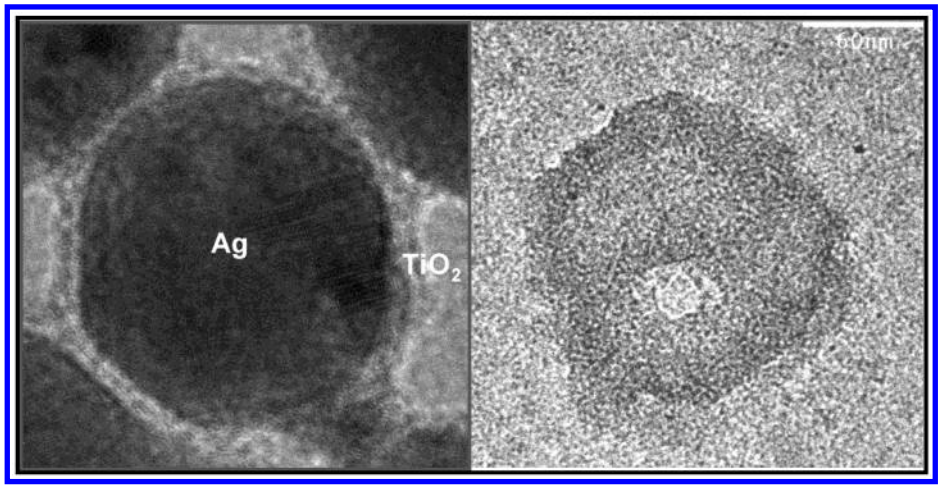

Figure 2. HRTEM images of $Ag@TiO_2$ nanoparticles before (left) and after (right) dissolution with ammonia. Adapted with permission from ref 64 (copyright, Wiley−VCH, 2002).

Few accounts have been published that are related to the coating of semiconductor nanocrystals with silica. Such a coating can serve not only to eliminate surface defects, but also to greatly enhance the stability, especially in aqueous solvents. A first report on the preparation of $CdS@SiO_2$ was published by Asher et al.,[54] using the microemulsion method. More recently, Correa-Duarte et al.[55] extended the silane coupling method that was previously developed for metals,[32] to link silica to the surface of CdS. The presence of the silica shell was shown to render the CdS cores stable against photodegradation.[55] A variation of this method was later used by Alivisatos et al.[56] to coat highly luminescent CdSe@CdS or CdSe@ZnS, for application as fluorescent biological labels. The same group performed a detailed study of the multistep coating process,[57] showing that there is plenty of colloid chemistry behind it, and that it can be applied to quantum dots of different sizes without a significant damping of the luminescence intensity, so that the labeling efficiency can be very high.

The same method with slight modifications was used by Rogach et al.[58] for the coating of CdTe and CdSe@CdS nanocrystals, which resulted in the inclusion of multiple cores within every silica sphere, yielding "raisin bun"-type nanoparticles. In this case, the luminescence intensity decreased dramatically during silica deposition.

Recently, Weller's group reported[59] the synthesis of water-soluble, silica-coated CdTe nanocrystals also using coupling agents, and their conjugation with biomolecules that provide molecular recognition potential (biotin/avidin or DNA).

2.2. Coating of Metal Nanocrystals with Semiconductors. The coating of metal nanoparticles with semiconductor shells is not directed, in general, to stability enhancement, but rather to obtain special properties due to the combination of two materials with different electronic structures. Kamat and Shanghavi[60] reported the preparation of Au@CdS nanoparticles by the surface modification of gold colloids with mercaptonicotinic acid, followed by addition of Cd^{2+} cations and exposure to H_2S. The result was the formation of very small CdS particles that were attached to the surface of the gold cores. Nayral et al. prepared $Sn@SnO_2$ particles to be used as potential gas sensors.[61] The core was allowed to undergo complete oxidation to form pure tin dioxide particles. With a view to conferring novel optical properties on particles, Nayak and others[62] generated Au@CdSe particles in organic solvents, although a large proportion of particles were a mixture of individual gold and CdSe particles, as detected by transmission electron microscopy (TEM).

Pastoriza-Santos et al.[63] synthesized $Ag@TiO_2$ particles by a modification of the procedure previously used for the synthesis of $Ag@SiO_2$ in DMF.[51] In this case, the reduction of $AgNO_3$ took place in DMF/ethanol mixtures in the presence of titanium tetrabutoxide, which condensed as TiO_2 on the surface of the silver cores. Dissolution of the silver cores with ammonia subsequently led to the formation of nanoshells, which can have significant applications[64] (see below). Figure 2 shows high-resolution TEM micrographs of one $Ag@TiO_2$ nanoparticle and one TiO_2 nanoshell, obtained through ammonia dissolution of the core.

The coating of gold nanoparticles with titania was also achieved by Mayya et al.,[65] using a different TiO_2 precursor (titanium(IV) bis(ammonium lactato) dihydroxide), which is negatively charged and readily complexes with a positively charged polyelectrolyte, poly(dimethyldiallylammonium chloride), that had been previously assembled on the nanoparticle surface. Upon complexation on the surface, controlled hydrolysis can be performed, thus providing good control of the morphology of the shell. The same authors applied this procedure to coat nickel nanorods with titania,[66] and upon dissolution of the nickel cores, they were able to obtain uniform TiO_2 nanotubes.

An interesting application of metal nanocrystals surrounded by semiconductor shells is the fabrication of composite nanoparticles with a large electronic capacitance. The idea is that there is a large difference between the Fermi level of the core and the conduction band energy of the semiconductor shell, so that electrons diffusing through the shell can be trapped in the core for long periods of time. Oldfield et al.[67] explored this possibility with gold nanoparticles encapsulated in a polycrystalline SnO_2 shell. These authors demonstrated that electrons can be injected by reducing radicals that are created homogeneously within the colloid, using γ-ray radiolysis. Electron injection via eq 4 resulted in a blue shift of the surface plasmon band, as predicted by the simple Drude theory.[68] The band remained blue-shifted in the absence of oxygen but slowly red-shifted back when exposed to air, because of oxygen reduction by the electrons that were stored in the core. The number of electrons stored on each 15-nm gold core was estimated to be as high as 1500−2000, as calculated from the blue shift of the surface plasmon band and independently from the discharge of the colloid capacitors, using zwitterionic viologen as an electron acceptor (eq 5). Figure 3 shows a high-resolution TEM image of one $Au@SnO_2$ nanoparticle, as well as the effect of oxygen addition upon cathodic polarization of the nanoparticles. Here, the shell increases the overpotential for

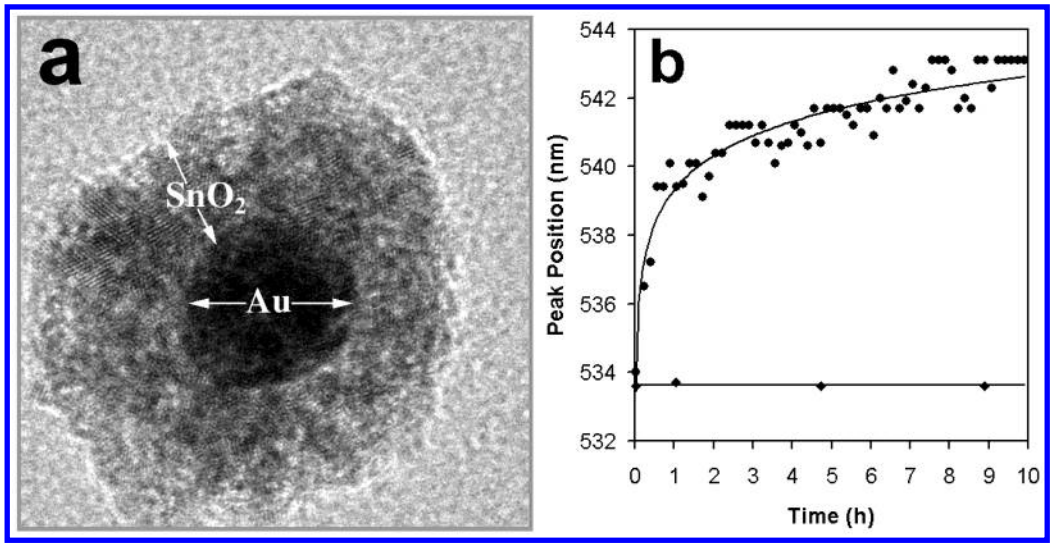

Figure 3. (a) HRTEM image of a 15-nm gold nanoparticle coated with polycrystalline SnO_2 (average thickness of 10 nm). (b) Plot showing the effect of oxygen (solid circles) on the position of the plasmon band of $Au@SnO_2$ nanocapacitors, which have been cathodically polarized by radiolytically generated CH_3CHOH radicals. As a reference, the plasmon band of the same sample stored under nitrogen (solid diamonds) is plotted over the same period of time. Adapted with permission from ref 67 (copyright, Wiley−VCH, 2000).

hydrogen formation, allowing more electrons to be stored within the core−shell structure.

$$n(CH_3)_2COH + Au@SnO_2 \rightarrow Au^{n-}@SnO_2 + n(CH_3)_2CO + nH^+ \quad (4)$$

$$Au^{n-}@SnO_2 + nZV \rightarrow Au@SnO_2 + nZV^- \quad (5)$$

3. Assembly of Coated Nanocrystals into Thin Films

The assembly of nanocrystals into ordered 2D arrays is quite difficult, because, as the particle size becomes smaller, capillary forces at the air−water interface and increased Brownian motion make crystallization processes more difficult. Initial methods for creating macroscopic 2D nanoparticle arrays used modified Langmuir Blodgett (LB) film techniques. Fendler, Kotov, and colleagues[69] nucleated the particles themselves directly beneath surfactant monolayers and then compressed them into ordered structures. This method was applied to a wide range of metal,[70] semiconductor,[71] and magnetic materials,[72] and the resultant particulate films could be transferred to a solid substrate. A high degree of order was obtained for magnetite monolayers that were prepared by the adsorption of magnetite nanocrystals underneath a floating layer of surfactant (stearic acid) from an aqueous subphase.[73] Alternatively, the particles can be synthesized in solution and rendered hydrophobic using the physisorption or chemisorption of surfactants, and these derivatized particles can be compressed within the LB trough. Capped or derivatized particles can also contain terminal functionalities that permit them to bond covalently to other surfaces. Alivisatos and co-workers bonded CdSe nanocrystals to both gold and aluminum surfaces.[74] Bawendi et al. used a modified LB procedure to fabricate submonolayers of capped CdSe nanocrystals that were bound to substrates.[75]

An alternative concept is to drive the particles to the surface, either electrically or magnetically. Electrophoretic deposition was used to deposit 15-nm citrate-stabilized gold nanocrystals onto a carbon-coated TEM grid.[76] This permitted direct observation of the 2D arrays in the electron microscope, and electron diffraction confirmed hexagonal close packing. The interparticle spacing could be controlled by alkanethiols of various chain lengths and by tuning the particle size. The same procedure was also used by Giersig et al.[77] to assemble similar gold nanocrystals that were coated with silica. The advantage of this system is that the interparticle separation is fully determined by the thickness of the silica shell. Electrophoresis also was applied to the deposition of PVP-stabilized platinum particles on electrodes,[78] showing a reasonable degree of order. Giersig and co-workers also demonstrated the possibility of using magnetic fields to assemble magnetic nanoparticles into highly ordered monolayers.[79,80]

Natan et al. showed that the self-assembly of gold and silver nanoparticles on polymer-coated substrates with thiol or amino functionalities leads to nanoparticle arrays that are highly active for surface-enhanced Raman scattering (SERS).[81] A similar procedure was used by Cotton et al.,[82] who attached gold and silver nanoparticles onto glass and quartz surfaces that had been derivatized with a mercaptosilane, yielding assemblies with unusual optical properties[83] that arise from coupling of the plasmon resonances of neighboring nanoparticles. Derivatization with other functionalities was also used by other authors.[84−87]

Pileni and co-workers reported the spontaneous formation of 2D arrays on surfaces that had been dipped into colloidal solutions of alkanethiol-capped particles.[88,89] In this case, the hydrophobicity of the immersed surface is a critical parameter that determines the efficiency of the transfer process. Researchers within the same group observed the self-assembly of magnetic cobalt nanoparticles that had been prepared within micelles.[90] Evidence was adduced for the collective magnetization flipping of magnetic moments within adjacent nanoparticles. The assembly of thiol-capped metal particles into monolayers was also studied by Heath's group, who reported phase diagrams[91,92] as well as the formation of mesoscopic rings formed from ordered nanoparticles.[93]

One method that has recently become very popular is layer-by-layer assembly (usually termed LBL). This procedure was originally developed for oppositely charged, micrometer-sized particles;[94] it was later extended to polyelectrolyte pairs.[95] LBL is based on the sequential dipping of a substrate into solutions (dispersions) of oppositely charged species.[96−101] It produces multilayer assemblies that are held together by the combination of attractive electrostatic and dispersive forces.[102] Alternating layers of positively and negatively charged components are the key components in LBL. The presence of a considerable surface

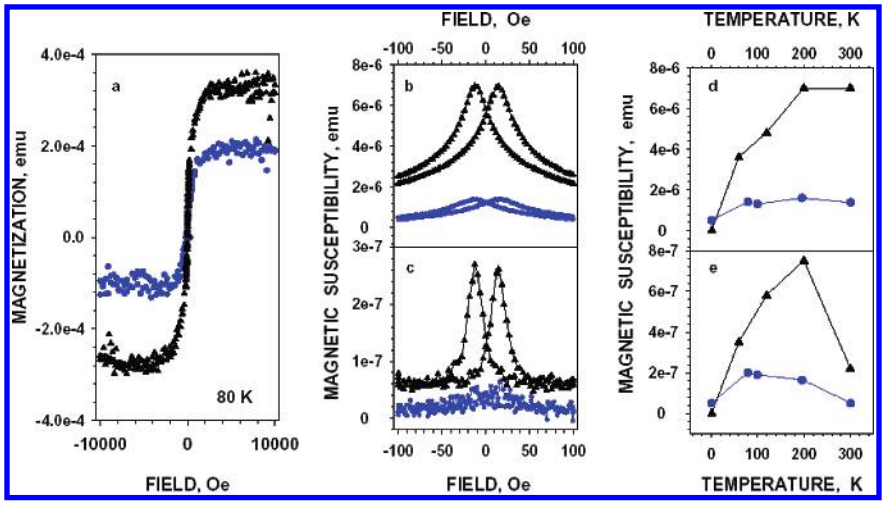

Figure 4. Magnetic properties of 10-layer LBL films from (●) silica-coated and (▲) noncoated magnetite: (a) hysteresis loops, (b,c) temperature dependence, and (d,e) magnetic field dependence of in-phase and out-of-phase components of magnetic susceptibility. Reproduced with permission from ref 29 (copyright, Wiley−VCH, 1999).

charge ensures the virtually monomolecular nature of the films, because of electrostatic repulsion between the newly formed layer and the free particles in solution. LBL films possess very homogeneous distributions of the components, even quite dissimilar ones, such as nanoparticles and polyelectrolytes.

In the remainder of this section, we demonstrate the use of LBL for the preparation of monolayers and multilayers of core−shell nanoparticles with three examples.

3.1. Fe_3O_4@SiO_2 Thin Films. It has been demonstrated[26,103] that LBL deposition affords the production of closely packed films of magnetic nanoparticles. The interest in this technique as an alternative to traditional deposition methods, such as sputtering and vacuum evaporation, stems from the soft conditions that are used (low temperature) and from the possibility to modify the particle size and morphology prior to the assembly. In the context of this review, the importance of this procedure is that it offers the possibility to coat individual magnetic grains with different materials, which may allow the controlled decoupling of magnetization switching in adjacent nanoparticles. A substantial reduction of media noise has been previously achieved in films with partial magnetic isolation of grains,[104,105] and the utilization of pre-made nanoparticles allows control and optimization of the domain size and shell thickness, as well as substantial improvement in the size distribution of the particles that comprise magnetic media.

Superparamagnetic Fe_3O_4 nanocrystals have been used[29] as a model system to demonstrate the LBL assembly of magnetic nanoparticle thin films and to investigate the effect of silica coating on the magnetic properties of such films. The effect was observed, on one hand, as a decrease in the saturation magnetization for the films made with silica-coated magnetite with the same number of monolayers (see Figure 4a). This was attributed to a surface-enhanced magnetic moment[106,107] in noncoated particles, while silica coating relaxes the surface stress and eliminates poorly coordinated surface iron bonds. This, in turn, reduces the total spin and decreases the magnetic moment of nanoparticles in the LBL film. On the other hand, measurements of the temperature dependence of the in-phase and out-of-phase magnetic susceptibility and the dependence of susceptibility in the presence of an applied field (Figure 4b, c) showed that there is an additional effect due to the screening of interparticle interactions when the magnetite nanoparticles are surrounded by an insulating silica shell. The thin SiO_2 layer produces an electron tunneling barrier between the magnetite cores, which impedes interparticle exchange interactions. Magnetic dipole coupling should be reduced to a smaller extent, because of the long-range nature of these forces. The disruption of the electronic communication between nanoparticles eliminates cooperative magnetization switching in which the magnetic reversal of one particle induces reorientation of the magnetic moment in numerous neighboring grains.[108] This results in a reduction of all components of the magnetic susceptibility and a corresponding decrease in noise.

3.2. Au@SiO_2 Thin Films. Another example that shows the role of silica coating on the control of collective properties of nanoparticles assembled as thin films can be found in silica-coated gold. In this case, the relevant properties are not magnetic; they are optical and related to the surface plasmon resonance of metal nanoparticles, which, for gold and other metals, leads to intense and well-defined absorption at visible wavelengths.[109] The optical properties of metal nanoparticles at low concentration can be calculated by means of a combination of the Mie theory and the Drude model.[68] However, when the concentration becomes higher, other models, such as effective medium theories,[110,111] need to be used, and, to test such theories, it is necessary to have a system that allows good control over interparticle separation. The LBL of Au@SiO_2 offers the possibility of controlling the particle volume fraction by means of the variation of the silica shell thickness, provided that the assembled films are close-packed.[112] Under close-packing conditions, the separation between the metal cores is just twice the thickness of the coating shell, which can be controlled during the synthesis of the colloids.

In Figure 5, the experimental absorbance and reflectance spectra, as well as selected photographs, are shown for thin films with different volume fractions of gold. As the volume fraction of gold increases (the separation between nanoparticles decreases), a red shift of the plasmon resonance is observed, as well as a broadening of the band. This effect originates in the dipole−dipole interactions between neighboring nanoparticles, and we can see here that a separation of just 15 nm is sufficient to screen such interactions, so that the thin films display basically the same properties as a dilute dispersion of the same nanoparticles in water.

Agreement between the experimental results and calculated spectra using Maxwell-Garnett effective medium theory[110] has been demonstrated, showing that this theory effectively accounts for dipole−dipole interactions.[112,113] Thus, both the transmission

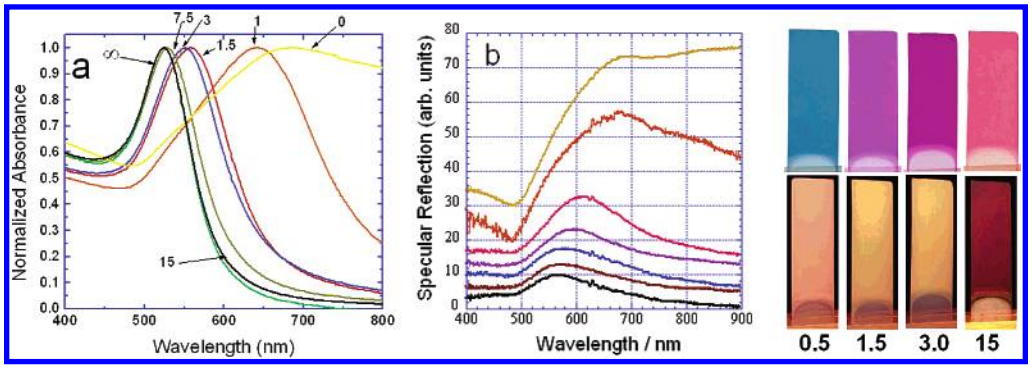

Figure 5. (a) Experimental absorbance and (b) reflectance spectra of Au@SiO_2 multilayer films as a function of the interparticle distance, as indicated (values given in nanometers). Images to the far right are selected photographs of the corresponding transmitted colors (top) and reflected colors (bottom). The numbers indicate shell thickness.

and reflection properties of thin gold films can be easily controlled by means of an adjustment of the thickness of the silica shell surrounding each nanocrystal. There is an important, as yet unexplored, aspect of the dipole coupling in these films. In principle, both the optical coupling of the surface plasmon modes and the van der Waals interactions between the gold nanocrystals share a common origin. As the particles approach each other, polarization of the conduction electron oscillations in adjacent particles causes the slow red shift in the plasmon frequency. This corresponds to a reduction in the free energy of the system. Coupling occurs when the particles are less than a diameter apart. The van der Waals interaction involves the same mechanism. The attractive force occurs because of correlated polarization between particles. In fact, the decrease in surface plasmon energy may be considered to be a direct measure of the reduction in energy of the coupled system of particles, because of van der Waals attraction. In other words, two approaching gold nanocrystals will change color as they collide, as a result of this electronic polarization. Because these color fluctuations occur on the time scale of individual Brownian encounters (milliseconds), they are not readily observed in solution; however, recent experimental approaches that allow the spectra of single gold particles to be recorded on surfaces may allow this relationship to be quantified for the first time.[114]

The LBL method can also be used for the assembly of nanoparticles on suitable colloid particles. This procedure has been developed by Caruso et al.[115,116] for a great variety of materials, a subject which has been recently reviewed.[117] This procedure has been also applied to the assembly of Au@SiO_2 nanocrystals on spherical polystyrene latex colloids.[118] The optical effects observed for the macroscopic thin films are now obtained for colloid particles, which, themselves, also possess a core−shell geometry, so that they can be used, in turn, for the construction of more complex, nanostructured materials. It has been found that silica-coated nanoparticles perform notably better for the formation of close-packed monolayers than other techniques that have been devised for the assembly of metal particles on colloid spheres.[119−121] The resulting spheres are essentially different to continuous metal shells that have been grown on colloid templates, which have been reported by Halas and colleagues[122,123] and by Graf and van Blaaderen.[124] Such continuous shells display optical properties that are associated with resonances of the entire shell and are, therefore, extremely sensitive to both core size and shell thickness, whereas, for the LBL-assembled Au@SiO_2, the optical properties are dependent only on the nature and dimensions of the constituents.

The assembly was initially performed for Au@SiO_2 with very thin shells (ca. 2 nm) on 640-nm polystyrene spheres[118] and later extended to latex cores of various sizes and gold nanoparticles that had been coated with thicker shells.[125] Examples of nanostructured colloids formed by assembly of Au@SiO_2 with identical cores but silica shells with various thicknesses are shown in Figure 6. It is clear that, although the surface of the particles is rough, the resultant coating layers are very compact and uniform, so that, again, the interparticle separation will be determined by the corresponding thickness of the silica shell. The experimental UV−visible spectra of 640-nm polystyrene colloids coated with five monolayers of Au@SiO_2 nanoparticles of various shell thickness are shown in the same figure. Again, as the separation between gold nanoparticles increases, the plasmon resonance blue-shifts toward that characteristic of isolated gold nanoparticles. As opposed to assemblies of the same coated nanoparticles on flat substrates, it has also been observed in the present case that the short-wavelength tail of the spectra rises dramatically as the size of the deposited nanoparticles increases, which is due to light scattering by the larger composite spheres.

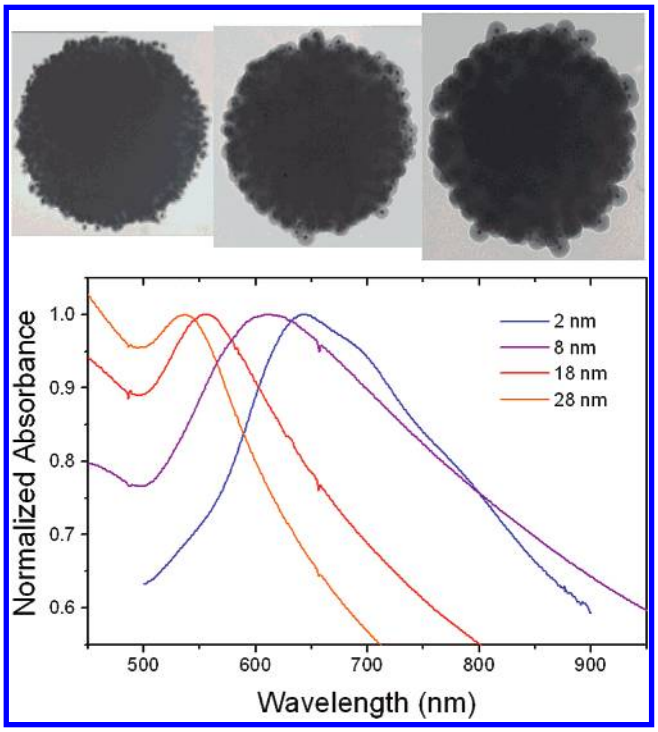

Figure 6. (Top) TEM micrographs of 640-nm polystyrene spheres on which one monolayer of Au@SiO_2 nanoparticles has been assembled. The size of the gold cores is 15 nm in all cases. From left to right, the silica shell thicknesses are 8, 18, and 28 nm. (Bottom) Normalized UV−visible spectra of dilute dispersions of 640-nm latex spheres coated with five monolayers of Au@SiO_2 nanoparticles with different shell thickness, as indicated.

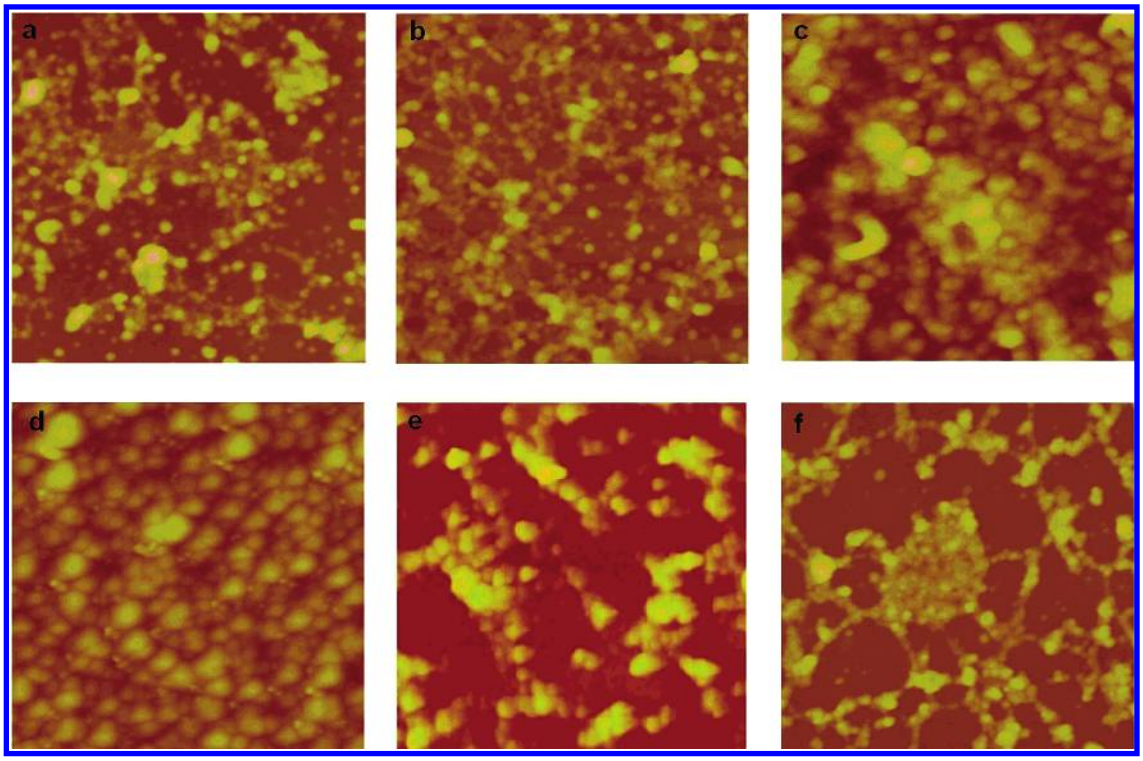

Figure 7. AFM images (1 μm × 1 μm) of monolayers of the nanoparticles shown in Figure 2a, assembled from dispersion at various pH ((a) 3.5, (b) 3.0, (c) 2.5, (d) 2.0, (e) 1.5, and (f) 1.0).

Calcination of the core−shell particles shown in Figure 6 leads to sintering of the silica shells, so that they become more stable, but also leads to the combustion of the polystyrene spheres, so that hollow Au−SiO_2 shells are finally obtained.[118] Such hollow spheres are extremely interesting for the construction of photonic materials with a large dielectric contrast. In addition, it is also possible to remove the insulating silica shells by gentle dissolution with hydrofluoric acid, so that shells made of closely packed gold nanoparticles are obtained.[125]

3.3. Hollow TiO_2 Thin Films. The possibility of conducting chemical reactions on the cores of coated particles has been demonstrated for Au@SiO_2 and Ag@SiO_2,[36−38] which is due to the porosity of the shells. For instance, the oxidation of metal cores by ammonia or cyanide in aqueous solution leads to the formation of hollow silica shells. This concept has also been recently exploited[64] to create nanostructured thin films made of hollow titania nanoshells, which were shown to be biocompatible and to exhibit interesting ion-sieving properties, which have been utilized for the selective detection of neurotransmitters.

The assembly process in this case was actually performed using Ag@TiO_2 nanoparticles synthesized in a mixture of DMF and ethanol.[63] After dilution with water at pH <3.5, the titania-coated particles became positively charged, whereas the large amount of dilution water activated the hydrophobic attraction to the polyelectrolyte strands. The surface density of nanoparticles was varied by changing the pH of the nanoparticle dispersions, as shown by atomic force microscopy (AFM) (Figure 7), with the best ordering observed at pH 2.0, which is the pH at which the nanoparticles formed densely packed films.

For the preparation of nanoshells, the silver cores were removed by adding a concentrated solution of ammonia (see Figure 2) to Ag@TiO_2 multilayer films. No difference in particle packing was observed before and after removal of the silver core. The existence of pores in TiO_2 nanoshells of sufficient size for Ag^+ ions to escape during oxidation and the hollow sphere geometry are indicative of the ion-sieving capabilities of this nanomaterial, which were demonstrated using cyclic voltammetry with potassium ferricyanide ($Fe(CN)_6^{3-}$) as a probe molecule. Ion permeability of the LBL nanoshell films is strongly dependent on pH and ionic strength, which permitted control of the diffusion just by adjusting these parameters. This is related to charge reversal within the nanoshells when the pH changes, thus allowing or excluding the diffusion of ions of a certain sign.

The biocompatible nature of this material, together with the strong ion selectivity, makes it a suitable candidate for neurotransmitter detection. An example of this application was shown in the selective enhancement of the permeation of positively charged dopamine, one of the most important neurotransmitters, and retardation of the transport of negatively charged ascorbic acid. Currently, the lack of dopamine/ascorbic acid selectivity for electrochemical in vivo detection of dopamine presents a significant problem for monitoring brain activity and for diagnostics of Parkinson's and similar neurological diseases.[126,127] The utilization of the nanoshell coatings enables a significant improvement in dopamine selectivity by suppressing the interference from oppositely charged electroactive ions.

4. Doped Glass from Coated Nanoparticles

The use of glass doped with metal nanoparticles for the construction of materials with nonlinear optical properties has long been studied. Most of the methods that have been used for the doping of glasses involve the reduction of infiltrated metal salts within the wet or dry gel. Although successful in most cases, such methods do not permit adequate control of the particle size and shape, or modification of the nanoparticle composition through alloying, for example.[128] These difficulties can be overcome if pre-made nanoparticles are incorporated into the glass matrix.

It was recently demonstrated[129,130] that silica-coated nanoparticles are ideal candidates for the fabrication of silica gels

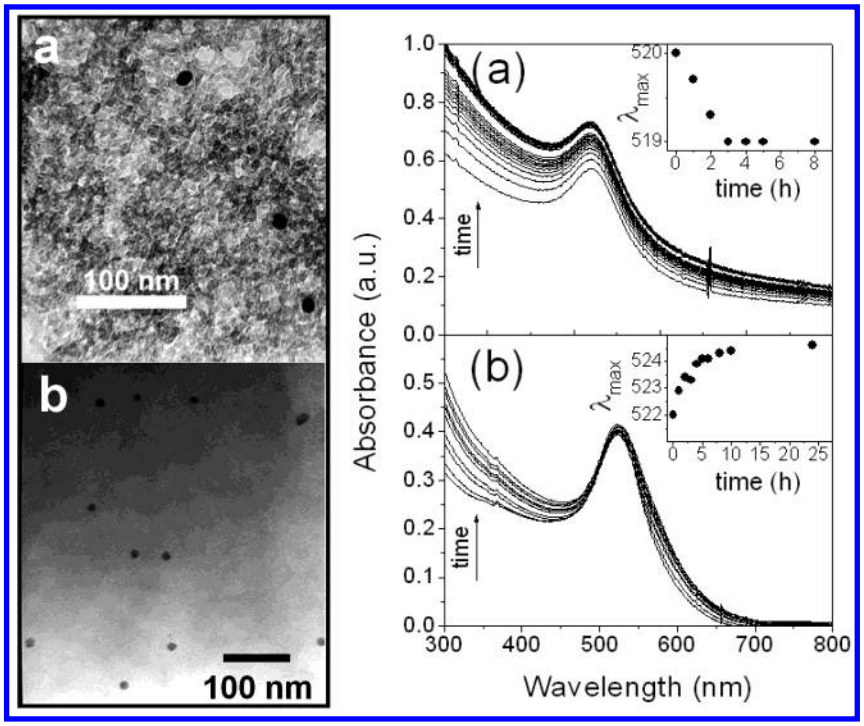

Figure 8. TEM micrographs (left) of silica gels doped with Au@SiO_2 nanoparticles prepared by sol−gel transition with (a) sodium silicate and (b) TMOS, and graphs (right) showing the time evolution of UV−visible spectra of Au@SiO_2 colloids during the sol−gel transition with (a) sodium silicate and (b) TMOS. Insets in graphs show the change in position of the plasmon resonance during the process.

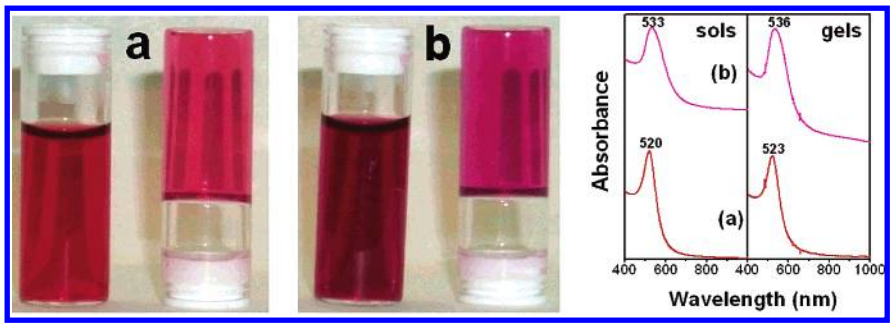

Figure 9. Photographs (left and center) and UV−visible spectra (right) of sols and gels doped with Au@SiO_2 nanoparticles with a shell thickness of 10 nm and core diameters of (a) 15 and (b) 30 nm. The position of the plasmon band is indicated.

and glasses that have been homogeneously doped with different types of nanoparticles. The reason for this is that the silica shell provides the core−shell nanoparticles with precisely the same surface properties as those of the silica units that are assembled during the sol−gel process, so that they do not have any preferred tendency to mutual coagulation and, thus, will be randomly distributed within the final nanostructure.

Doped silica gels can be prepared by simply mixing colloids with sodium silicate, followed by careful neutralization of the basic solution;[15] however, this leads to the formation of relatively large pores (Figure 8a) and, consequently, to more turbid materials. Better glasses for optical applications can be prepared by performing the sol−gel process through the controlled hydrolysis of tetramethoxysilane (TMOS),[131] as shown in Figure 8b. The different light scattering intensity from both gels is reflected in the increased absorbance at low wavelengths, as shown in Figure 8. The concentration of the nanoparticles within the gels can be varied by simple adjustment of the concentration of the colloid prior to the sol−gel process.[129]

Because silica coating has been demonstrated for several nanoparticles with different composition, size, and shape (see previous discussion), the use of silica-coated nanoparticles offers an almost unlimited range of possibilities for the synthesis of doped gels and glasses with various properties. In Figure 9, an example of gels prepared from silica-coated gold with two different sizes is shown, demonstrating that the optical properties are preserved during the sol−gel transition.

The third-order nonlinear optical properties of such gels have been measured[132] by degenerate four-wave mixing. This yields values for the third-order susceptibility, $|\chi^{(3)}|$, from the measurement of the intensities of incident, transmitted, and signal beams, at a wavelength close to the maximum of the surface plasmon band. For a thin xerogel containing 0.14 wt % gold, the measured value of $|\chi^{(3)}|$ was 2.3×10^{-10} esu, whereas, after sintering at 600 °C to convert the xerogel to a glass, the $|\chi^{(3)}|$ value was 4.6×10^{-10} esu. These values are more than 10 times larger than those of gold particles in glasses prepared by the conventional melt-quenching method,[133] and demonstrate the usefulness of this very simple synthetic procedure for the fabrication of materials with interesting optical properties.

5. Ordered Nanocrystal Assemblies

5.1. Au@SiO_2 Opals. One of the objectives behind the assembly of colloidal particles into ordered structures is the achievement of a periodically modulated dielectric constant, which is the basis for the preparation of photonic crystals.[134]

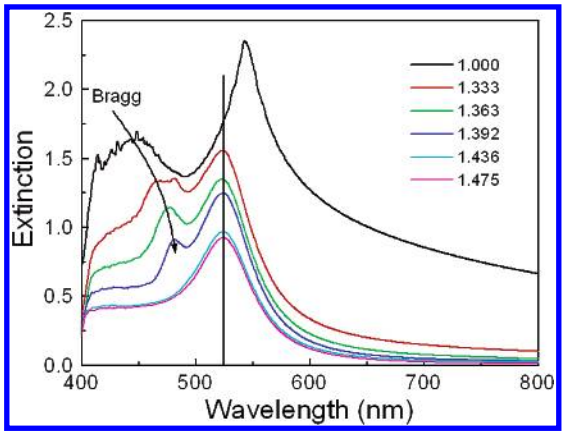

Figure 10. Extinction spectra in different media (air, water, and water−glycerol mixtures) for sintered opals made of Au@SiO_2 particles with a core diameter of 15 nm and a total diameter of 225 nm. The corresponding refractive indices are indicated.

One example of such structures can be found in a natural material, the opal,[135] and scientists are searching for procedures to imitate nature and produce artificially crystalline structures from monodisperse colloid particles.[136] The main difficulty is achievement of a sufficiently high refractive index contrast between the particles and the voids.[137] However, theoretical calculations show that crystals with face-centered-cubic (fcc) structures,[138] and especially diamond or zinc blende lattices[139] of metal spheres with a dielectric coating, have wide photonic band gaps, originating from the large, negative value of the real part of the dielectric constant. Although absorption arising from the imaginary part of the dielectric constant of the metal could destroy the band gap, for the noble metals, the absorption will be small enough to make such photonic crystals useful at frequencies in the visible and near-IR regions, with silver performing the best.[140]

One simple route to opal formation is slow sedimentation of the colloid particles in a suitable solvent, so that the interparticle interactions during deposition result in ordered structures with an fcc crystal lattice.[141] The same method can be applied to the formation of opals using Au@SiO_2 particles as the constituent units,[142] because the nature of the surface is identical. The optical characterization of such opals suggests that the plasmon resonance and Bragg diffraction are altered through independent mechanisms. Clear evidence for this is shown in Figure 10, where optical extinction spectra have been plotted for a single Au@SiO_2 opal, but with different materials filling the interstices between the spheres. Although the position of the Bragg peak is red-shifted and its intensity is reduced as the refractive index of the medium is increased (and the optical contrast is accordingly reduced), the plasmon band position remains basically unchanged, because the silica shell around the gold cores is thick enough that they do not "see" the outer medium any longer.

The major requirement for long-range ordering is that the particles experience repulsive interactions or attractive interactions of $\sim kT$. However, van der Waals forces between nanocrystals are already much greater than kT (see Table 1), so that this process is possible only for nanocrystals that have been stabilized by repulsive interactions, which can offset the attractive interactions that would otherwise produce disordered or fractal-like structures. Nanocrystals that experience repulsive interaction forces will spontaneously order when subjected to a cohesive pressure. The difficulty arises that, after the pressure is released, the system disorders. For example, centrifugation can lead to the ordering of very small colloid particles; however, thermal diffusion rapidly disrupts the structure after the field is switched off. What is needed is a method to apply a cohesive force after ordering. One approach is to induce ordering and then use sol−gel processing to lock the structure into place. In Figure 11, we show scanning electron microscopy (SEM) micrographs of Au@SiO_2 particles that have been sedimented in ethanol using a 3-(trimethoxysilyl)propyl methacrylate (TPM) coating. Ammonia and TMOS were then injected and the centrifugation was continued.[143] The TMOS hydrolysis occurs over a time span of approximately an hour, and the oligomeric silanes bridge the colloidal opal. Solvent is displaced gradually, although not completely. The gelation can be accelerated using an alkylamine. The resultant opal is a deep transparent red color, because diffraction from the periodic gold nanocrystal lattice occurs in the UV region. The method yields single crystals several hundred micrometers in size, as determined by small-angle X-ray scattering (SAXS).

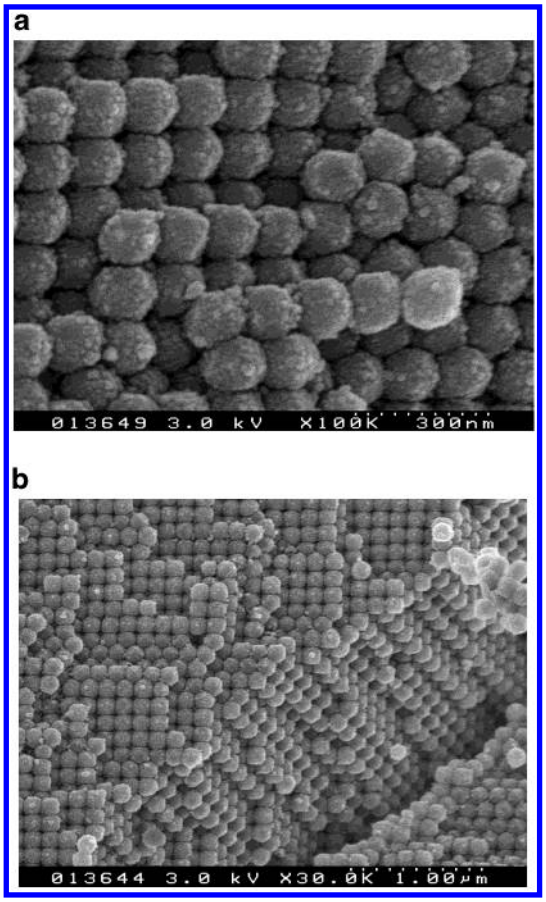

Figure 11. (a) Large-scale face-centered-cubic (fcc) Au@SiO_2 lattice created by simultaneous sol−gel processing and centrifugation using TMOS, octylamine, and ethanol.[143] The sample has been fractured for SEM imaging. (b) Smaller blobs of condensed silane, which hold the opal together, can be observed on the surfaces of the spheres.

5.2. Inverse Opals from Au@SiO_2 Particles. One final example of nanostructures that have been created from the assembly of silica-coated nanocrystals is the formation of inverse opals. These structures are similar to opals, in the sense that they comprise solids with an ordered structure whose lattice constant lies in the optical wavelength range. The only difference lies in the nature of the crystal centers and the embedding medium. "Direct" opals are composed of solid (or liquid) particles typically embedded in air, whereas "inverse" opals are comprised of air bubbles embedded in a solid material. One of the most promising pathways toward the fabrication of inverse opals is the infiltration of the interstices of direct opals with

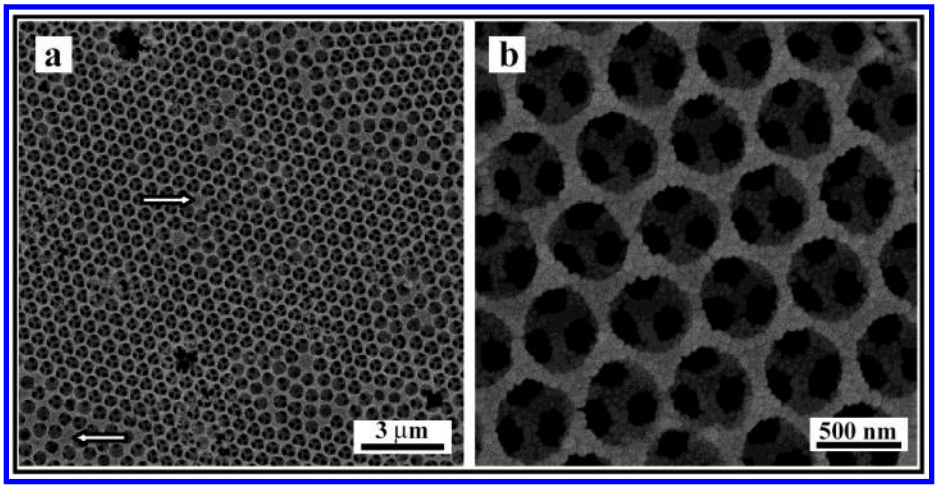

Figure 12. SEM micrographs ((a) low and (b) high magnification) of $Au-SiO_2$ inverse opals formed by infiltrating colloidal crystals made of polystyrene spheres (640 nm in diameter) with $Au@SiO_2$ nanoparticles (core diameter, 15 nm; shell thickness, 28 nm). Arrows in panel a show point defects within the crystalline structure. Adapted with permission from ref 147 (copyright, Wiley-VCH, 2002).

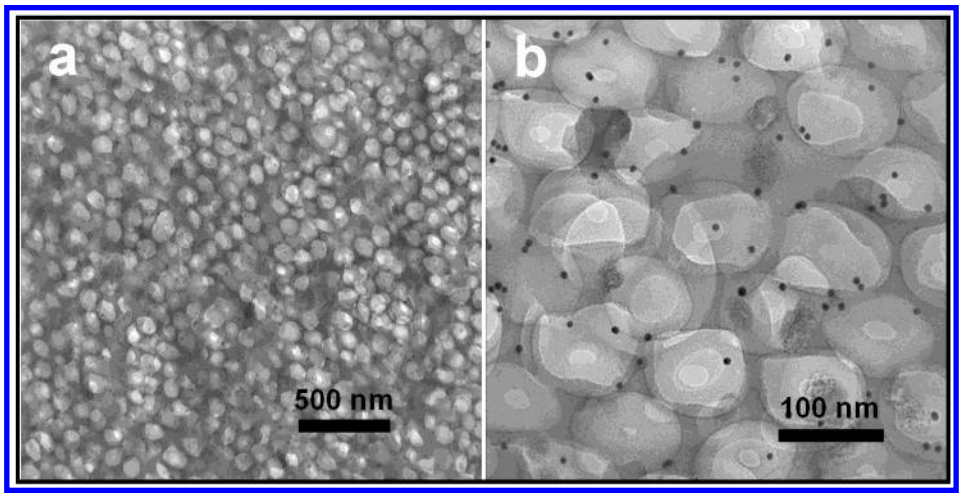

Figure 13. Electron micrographs showing (a) a large area and (b) a small area of an epoxy resin inverse opal with incorporated gold nanoparticles.

the desired material, followed by removal of the colloid templates.[144] Photonic crystals with a full photonic band gap in the IR region have been reported with the inverse opal structure for silicon[145] and germanium.[146] This is hard to achieve for visible wavelengths; therefore, the use of noble metals has been shown to favor the opening of a complete photonic band gap, even in a simple fcc structure.[138] It is therefore desirable to use metals with a well-defined plasmon frequency, which is the case for metal nanoparticles. Thus, one suitable approach is the infiltration of preformed opals with the previously described $Au@SiO_2$ nanoparticles, so that the optical features of single nanoparticles are preserved in the final inverse opal.[147] After the template is removed, rigid and mechanically stable nanostructures can be easily obtained through sintering of the silica shells, while retaining the optical properties of the individual gold nanoparticles. An example of $Au@SiO_2$-based inverse opals that have been prepared by the infiltration of polystyrene latex opals and template removal by calcination is shown in Figure 12. The figure contains low- and high-resolution SEM micrographs of an inverse opal formed by $Au@SiO_2$ nanoparticles with 15-nm gold cores that are surrounded by 28-nm-thick silica shells. The spherical particles can still be recognized within the nanostructured system. The optical characterization of these inverse opals shows again that the position of both the plasmon band and the Bragg peak can be modulated independently, so that a gate is open to search for the coupling that is needed to achieve a full photonic band gap.

Inverse opals of a different nature, but also synthesized through the assembly of $Au@SiO_2$ core−shell spheres, have been recently reported.[148] In this case, opals made from silica-coated gold nanoparticles with a total diameter of 225 nm were infiltrated with a curable epoxy resin. Upon curing of the resin at 70 °C and subsequent etching of the silica shells with hydrofluoric acid, an ordered macroporous polymer is obtained, within which gold nanoparticles were homogeneously distributed. Note that complete dissolution of the silica shells is only possible because of the contact between neighboring spheres, which is ensured through the sintering of the opal. Electron microscopy images showing the morphology of the resultant material are shown in Figure 13. It is clear that the ordered nature of the sacrificial opal is retained in the inverse structure; however, although the metal nanoparticles are homogeneously distributed within the porous material, they do lose their crystalline arrangement, because, as the silica shells are dissolved, they randomly stick to the closest wall available. The applications of such materials are not just in the field of photonics, but also in catalysis. Because of the connecting windows between neighboring air bubbles, the metal nanoparticles can be easily accessed when the porous solid is placed

within the medium where the reaction to be catalyzed is intended to take place.

Another corollary of the regular nanoporous nature of the inverse opal structure is that it is highly curved and the wettability of the material will be strongly determined by capillary forces. In fact, such materials are spongelike and will hold fluids against substantial reductions in vapor pressure. Consequently, they may also function as slow-release membranes or films, which may prove useful in drug delivery.

6. Nanomechanics

At the start of this review, we alluded to the fact that a major driving force for nanocrystal assembly is the desire to be able to modulate the intrinsic length scales of inorganic materials and, thereby, tune their electronic, mechanical, acoustic, and optical responses. Although most of the review has focused on the collective optical properties of these assemblies, an interesting question is the measurement of their mechanical properties, such as the Young's modulus of a photonic crystal that is composed of submicrometer-sized silica or core−shell nanocrystals. One hypothetical approach to this problem, based on recent work on measurement of the thickness dependence of the Young's modulus of gold films, is to use microfabricated levers or beams as measuring devices.[149] A rectangular AFM microcantilever in a vacuum vibrates at a frequency that is given by

$$f = 0.162(w/L^2)(E/\rho)^{1/2} \qquad (6)$$

where w is the width, L the length, E the Young's modulus, and ρ the beam density. Hence, if a photonic crystal is grown on a microcantilever, it is possible, in principle, to monitor its elastic modulus as it grows from changes in the resonance frequency of the cantilever. This provides important information on the particle−particle adhesive forces that are responsible for the mechanical properties of the nanocrystal assembly. The elastic properties determine the speed of sound in the resultant assembly and the eigenfrequencies of vibration. These are important parameters in the design of rigid, ductile, or elastic nanocrystal-based assemblies.

The topologies of the assemblies described in this review have been simple; the major gains to date have been in the increased uniformity of sphere preparation, enabling larger crystalline domains to be constructed through manipulation of the interparticle forces. Soon, intertwining of the colloid lattices may be possible, enabling the construction of controlled permeation structures, while the creation of macroscopic chiral materials through self-assembly is an important milestone. However, the next likely domain will be optomechanical (OM) structures. In OM materials, a variety of physical stimuli (such as compression, shear, torsion and extension, electrical currents, or pressure) will induce optical changes in materials, such as fluorescence or color modulation. This is a fundamental mechanism that is important for the design of smart textiles, bionic circuitry, responsive environmental sensors, and general signal transduction elements.

7. Conclusions and Outlook

In this article, we have described the use of core−shell nanoparticles for the construction of functional, nanostructured materials. In the examples that were chosen for more detailed discussion, it was shown that careful control of the thickness of the insulating shells can provide sensitive tuning of the global response of the system toward external actions, such as incoming light or applied magnetic fields. Furthermore, it was shown that gold nanoparticles can be randomly incorporated within silica gels, through sol−gel processing of the silica-coated nanoparticles, as well as the formation of three-dimensional, ordered arrangements of the coated metal particles, which sets a starting point for a more-detailed study of the coupling between surface plasmon resonance and Bragg diffraction.

The construction of nanostructures using core−shell nanoparticles that comprise semiconductor materials has not been discussed here; however, such construction does constitute, in itself, a broad and promising area that is already starting to be explored. Such coated particles can exhibit enhanced luminescence and chemical stability, so that they constitute ideal candidates for the design of novel lasers and light-emitting displays, among a range of other practical devices.

Because of space limitations, we have also omitted organic and hybrid organic−inorganic core−shells; however, in the future, such composite materials will play an ever-increasing role.

Acknowledgment. The authors are indebted to the many students and collaborators who have actively contributed to the work described in this article.

References and Notes

(1) Russel, W. B.; Saville, D. A.; Showalter, W. R. *Colloidal Dispersions*; Cambridge University Press: Cambridge, U.K., 1989.
(2) Israelachvili, J. *Intermolecular and Surface Forces*, 2nd ed.; Academic Press: London, 1985.
(3) Beverly, K. C.; Sample, J. L.; Sampaio, J. F.; Remacle, F.; Heath, J. R.; Levine, R. D. *Proc. Natl. Acad. Sci. U.S.A.* **2002**, *99* (Suppl. 2), 6456.
(4) Remacle, F.; Beverly, K. C.; Heath, J. R.; Levine, R. D. *J. Phys. Chem. B* **2002**, *106*, 4116.
(5) Müller, K.-H.; Herrmann, J.; Raguse, B.; Baxter, G.; Reda, T. *Phys. Rev. B* **2002**, *66*, 075417.
(6) Larson, R. G. *The Structure and Rheology of Complex Fluids*; Oxford University Press: Oxford, U.K., 1999.
(7) Henglein, A. *J. Phys. Chem.* **1993**, *97*, 4657.
(8) Henglein, A. *Top. Curr. Chem.* **1988**, *113*, 149.
(9) Alivisatos, A. P. *Science* **1996**, *271*, 933.
(10) Murray, C. B.; Sun, S.; Doyle, H.; Betley, T. *MRS Bull.* **2001**, *26*, 985.
(11) Liz-Marzán, L. M.; Correa-Duarte, M. A.; Pastoriza-Santos, I.; Mulvaney, P.; Ung, T.; Giersig, M.; Kotov, N. A. In *Handbook of Surfaces and Interfaces of Materials*; Nalwa, H. S., Ed.; Academic Press: San Diego, CA, 2001; Vol. 3, pp 189−237.
(12) Verwey, E. J. W.; Overbeek, J. Th. G. *Theory of the Stability of Lyophobic Colloids*; Elsevier: Amsterdam, 1948.
(13) Allen, L. H.; Matijevic, E. *J. Colloid Interface Sci.* **1969**, *31*, 287.
(14) Depasse, J.; Watillon, A. *J. Colloid Interface Sci.* **1970**, *33*, 430.
(15) Iler, R. K. *The Chemistry of Silica*; Wiley: New York, 1979.
(16) Vigil, G.; Xu, Z.; Steinberg, S.; Israelachvili, J. *J. Colloid Interface Sci.* **1994**, *165*, 367.
(17) Küspert, F. *Berichte* **1919**, *35*, 2815.
(18) Furlong, D. N.; Freeman, P. A.; Lau, A. C. M. *J. Colloid Interface Sci.* **1981**, *80*, 21.
(19) Bergna, H. E. In *The Colloid Chemistry of Silica*; Bergna, H. E., Ed.; American Chemical Society: Washington, DC, 1994; pp 1−47.
(20) Iler, R. K. Product Comprising a Skin of Dense, Hydrated Amorphous Silica Bound Upon a Core of Another Solid Material and Process of Making Same. U.S. Patent No. 2,885,366, May 5, 1959.
(21) Philipse, A. P.; van Bruggen, M. P.; Pathmamanoharan, C. *Langmuir* **1994**, *10*, 92.
(22) Philipse, A. P.; Nechifor, A. M.; Pathmamanoharan, C. *Langmuir* **1994**, *10*, 4451.
(23) Ohmori, M.; Matijevic, E. *J. Colloid Interface Sci.* **1992**, *150*, 594.
(24) Stöber, W.; Fink, A.; Bohn, E. *J. Colloid Interface Sci.* **1968**, *26*, 62.
(25) Liu, Q.; Xu, Z.; Finch, J. A.; Egerton, R. *Chem. Mater.* **1998**, *10*, 3938.
(26) Correa-Duarte, M. A.; Giersig, M.; Kotov, N. A.; Liz-Marzán, L. M. *Langmuir* **1998**, *14*, 6430.
(27) Lu, Y.; Yin, Y.; Mayers, B. T.; Xia, Y. *Nano Lett.* **2002**, *2*, 183.
(28) Donselaar, L. N.; Philipse, A. P. *J. Colloid Interface Sci.* **1999**, *212*, 14.

(29) Aliev, F. G.; Correa-Duarte, M. A.; Mamedov, A.; Ostrander, J. W.; Giersig, M.; Liz-Marzán, L. M.; Kotov, N. A. *Adv. Mater.* **1999**, *11*, 1006.
(30) Ohmori, M.; Matijevic, E. *J. Colloid Interface Sci.* **1993**, *160*, 288.
(31) Liz-Marzán, L. M.; Philipse, A. P. *J. Colloid Interface Sci.* **1995**, *176*, 459.
(32) Liz-Marzán, L. M.; Giersig, M.; Mulvaney, P. *J. Chem. Soc., Chem. Commun.* **1996**, 731.
(33) Liz-Marzán, L. M.; Giersig, M.; Mulvaney, P. *Langmuir* **1996**, *12*, 4329.
(34) Plueddermann, E. P. *Silane Coupling Agents*; Plenum Press: New York, 1991.
(35) Liz-Marzán, L. M.; Mulvaney, P. *New J. Chem.* **1998**, 1285.
(36) Giersig, M.; Ung, T.; Liz-Marzán, L. M.; Mulvaney, P. *Adv. Mater.* **1997**, *9*, 570.
(37) Ung, T.; Liz-Marzán, L. M.; Mulvaney, P. *Langmuir* **1998**, *14*, 3740.
(38) Ung, T.; Liz-Marzán, L. M.; Mulvaney, P. *J. Phys. Chem. B* **1999**, 6770.
(39) Chang, S. S.; Shih, C. W.; Chen, C. D.; Lai, W. C.; Wang, C. R. *Langmuir* **1999**, *15*, 701.
(40) Obare, S. O.; Jana, N. R.; Murphy, C. J. *Nano Lett.* **2001**, *1*, 601.
(41) Hall, S. R.; Davis, S. A.; Mann, S. *Langmuir* **2000**, *16*, 1454.
(42) Hardikar, V. V.; Matijevic, E. *J. Colloid Interface Sci.* **2000**, *221*, 133.
(43) Yin, Y.; Lu, Y.; Sun, Y.; Xia, Y. *Nano Lett.* **2002**, *2*, 427.
(44) Lu, Y.; Yin, Y.; Li, Z.-Y.; Xia, Y. *Nano Lett.* **2002**, *2*, 785.
(45) Mine, E.; Yamada, A.; Kobayashi, Y.; Konno, M.; Liz-Marzán, L. M. *J. Colloid Interface Sci.*, in press.
(46) Yau, S.-T.; Mulvaney, P.; Xu, W.; Spinks, G. M. *Phys. Rev. B* **1998**, *57*, R15124.
(47) Makarova, O. V.; Ostafin, A. E.; Miyoshi, H.; Norris, J. R., Jr.; Meisel, D. *J. Phys. Chem. B* **1999**, *103*, 9080.
(48) Nooney, R. I.; Dhanasekaran, T.; Chen, Y.; Josephs, R.; Ostafin, A. E. *Adv. Mater.* **2002**, *14*, 529.
(49) Li, T.; Moon, J.; Morrone, A. A.; Mecholsky, J. J.; Talhman, D. R.; Adair, J. H. *Langmuir* **1999**, *15*, 4328.
(50) Martino, A.; Yamanaka, S. A.; Kawola, J. S.; Loy, D. A. *Chem. Mater.* **1997**, *9*, 423.
(51) Pastoriza-Santos, I.; Liz-Marzán, L. M. *Langmuir* **1999**, *15*, 948.
(52) Pastoriza-Santos, I.; Liz-Marzán, L. M. *Pure Appl. Chem.* **2000**, *72*, 83.
(53) Schärtl, W. *Adv. Mater.* **2000**, *12*, 1899.
(54) Chang, S.; Liu, L.; Asher, S. A. *J. Am. Chem. Soc.* **1994**, *116*, 6739.
(55) Correa-Duarte, M. A.; Giersig, M.; Liz-Marzán, L. M. *Chem. Phys. Lett.* **1998**, *286*, 497.
(56) Bruchez, M., Jr.; Moronne, M.; Gin, P.; Weiss, S.; Alivisatos, A. P. *Science* **1998**, *281*, 2013.
(57) Gerion, D.; Pinaud, F.; Williams, S. C.; Parak, W. J.; Zanchet, D.; Weiss, S.; Alivisatos, A. P. *J. Phys. Chem. B* **2001**, *105*, 8861.
(58) Rogach, A. L.; Nagesha, D. K.; Ostrander, J. W.; Giersig, M.; Kotov, N. A. *Chem. Mater.* **2000**, *12*, 2676.
(59) Schroedter, A.; Weller, H.; Eritja, R.; Ford, W. E.; Wessels, J. M. *Nano Lett.* **2002**, *2*, 1363.
(60) Kamat, P. V.; Shanghavi, B. *J. Phys. Chem. B* **1997**, *101*, 7675.
(61) Nayral, C.; Ould-Ely, T.; Maisonnat, A.; Chaudret, B.; Fau, P.; Lescouzères, L.; Peyre-Lavigne, A. *Adv. Mater.* **1999**, *11*, 61.
(62) Nayak, R.; Galsworthy, J.; Dobson, P.; Hutchinson, J. *J. Mater. Res.* **1998**, *13*, 905.
(63) Pastoriza-Santos, I.; Koktysch, D.; Mamedov, A.; Kotov, N. A.; Liz-Marzán, L. M. *Langmuir* **2000**, *16*, 2731.
(64) Koktysh, D. S.; Liang, X.; Yun, B.-G.; Pastoriza-Santos, I.; Matts, R. L.; Giersig, M.; Serra-Rodríguez, C.; Liz-Marzán, L. M.; Kotov, N. A. *Adv. Funct. Mater.* **2002**, *12*, 255.
(65) Mayya, K. S.; Gittins, D. I.; Caruso, F. *Chem. Mater.* **2001**, *13*, 3833.
(66) Mayya, K. S.; Gittins, D. I.; Dibaj, A. M.; Caruso, F. *Nano Lett.* **2001**, *1*, 727.
(67) Oldfield, G.; Ung, T.; Mulvaney, P. *Adv. Mater.* **2000**, *12*, 1519.
(68) Mulvaney, P. *Langmuir* **1996**, *12*, 788.
(69) Kotov, N. A.; Meldrum, F. C.; Wu, C.; Fendler, J. H. *J. Phys. Chem.* **1994**, *98*, 2735.
(70) Yi, K. C.; Sánchez Mendieta, V.; Lopez Castañares, R.; Meldrum, F. C.; Wu, C.; Fendler, J. H. *J. Phys. Chem.* **1995**, *99*, 9868.
(71) Kotov, N. A.; Meldrum, F. C.; Wu, C.; Fendler, J. H. *J. Phys. Chem.* **1994**, *98*, 2735.
(72) Zhao, X.; Xu, S.; Fendler, J. H. *J. Phys. Chem.* **1990**, *94*, 2573.
(73) Iakovenko, S. A.; Trifonov, A. S.; Giersig, M.; Mamedov, A.; Nagesha, D. K.; Hanin, V. V.; Soldatov, E. C.; Kotov, N. A. *Adv. Mater.* **1999**, *11*, 388.
(74) Colvin, V. L.; Goldstein, A. N.; Alivisatos, A. P. *J. Am. Chem. Soc.* **1992**, *114*, 5221.
(75) Dabbousi, B. O.; Murray, C. B.; Rubner, M. F.; Bawendi, M. G. *Chem. Mater.* **1994**, *6*, 216.
(76) Giersig, M.; Mulvaney, P. *Langmuir* **1993**, *9*, 3408.
(77) Giersig, M.; Liz-Marzán, L. M.; Ung, T.; Su, D.; Mulvaney, P. *Ber. Bunsen−Ges.* **1997**, *101*, 1617.
(78) Teranishi, T.; Hosoe, M.; Miyake, M. *Adv. Mater.* **1997**, *9*, 65.
(79) Giersig, M.; Hilgendorff, M. *J. Phys. D: Appl. Phys.* **1999**, *32*, L111.
(80) Hilgendorff, M.; Tesche, B.; Giersig, M. *Aust. J. Chem.* **2001**, *54*, 497.
(81) Freeman, R. G.; Grabar, K. C.; Allison, K. J.; Bright, R. M.; Davis, J. A.; Guthrie, A. P.; Hommer, M. B.; Jackson, M. A.; Smith, P. C.; Walter, D. G.; Natan, M. J. *Science* **1995**, *267*, 1629.
(82) Chumanov, G.; Sokolov, K.; Gregory, B. W.; Cotton, T. M. *J. Phys. Chem.* **1995**, *99*, 9466.
(83) Chumanov, G.; Sokolov, K.; Cotton, T. M. *J. Phys. Chem.* **1996**, *100*, 5166.
(84) Doron, A.; Katz, E.; Willner, I. *Langmuir* **1995**, *11*, 1313.
(85) Gilbert, S. E.; Cavalleri, O.; Kern, K. *J. Phys. Chem.* **1996**, *100*, 12123.
(86) Bright, R. M.; Musick, M. D.; Natan, M. J. *Langmuir* **1998**, *14*, 5695.
(87) Hu, K.; Brust, M.; Bard, A. J. *Chem. Mater.* **1998**, *10*, 1160.
(88) Motte, L.; Billoudet, F.; Lacaze, E.; Douin, J.; Pileni, M. P. *J. Phys. Chem. B* **1997**, *101*, 138.
(89) Motte, L.; Pileni, M. P. *J. Phys. Chem. B* **1998**, *100*, 4104.
(90) Petit, C.; Taleb, A.; Pileni, M. P. *J. Phys. Chem. B* **1999**, *103*, 1805.
(91) Heath, J. R.; Knobler, C. M.; Leff, D. V. *J. Phys. Chem. B* **1997**, *101*, 189.
(92) Ohara, P. C.; Leff, D. V.; Heath, J. R.; Gelbart, W. M. *Phys. Rev. Lett.* **1995**, *75*, 3466.
(93) Ohara, P. C.; Heath, J. R.; Gelbart, W. M. *Angew. Chem., Int. Ed.* **1997**, *36*, 1078.
(94) Iler, R. K. *J. Colloid Interface Sci.* **1966**, *21*, 569.
(95) Decher, G. *Science* **1977**, *277*, 1232.
(96) Kotov, N. A.; Dékány, I.; Fendler, J. H. *Adv. Mater.* **1996**, *8*, 637.
(97) Schmitt, J.; Decher, G.; Dressick, W. J.; Brandow, S. L.; Geer, R. E.; Shashidhar, R.; Calvert, J. M. *Adv. Mater.* **1997**, *9*, 61.
(98) Lvov, Y.; Ariga, K.; Onda, M.; Ichinose, I.; Kunitake, T. *Langmuir* **1997**, *13*, 6195.
(99) Donath, E.; Sukhorukov, G. B.; Caruso, F.; Davis, S. A.; Möhwald, H. *Angew. Chem., Int. Ed. Engl.* **1998**, *37*, 2201.
(100) Kotov, N. A.; Haraszti, T.; Turi, L.; Zavala, G.; Geer, R. E.; Dékány, I.; Fendler, J. H. *J. Am. Chem. Soc.* **1997**, *119*, 6821.
(101) Ollivier, P. J.; Kovtyukhova, N. I.; Keller, S. W.; Mallouk, T. E. *Chem. Commun.* **1998**, 1563.
(102) Ostrander, J. W.; Mamedov, A. A.; Kotov, N. A. *J. Am. Chem. Soc.* **2001**, *123*, 1101.
(103) Kotov, N. A. *Nanostruct. Mater.* **1999**, *12*, 789.
(104) Choe, G.; Chung, S. J.; Walser, R. M. *Thin Solid Films* **1995**, *259*, 231.
(105) Murayama, A.; Ohshima, K.; Miyamura, M.; Maekawa, M.; Kondoh, S. *J. Appl. Phys.* **1996**, *79*, 7916.
(106) Himpsel, F. J.; Ortega, J. E.; Mankey, G. J.; Willis, R. F. *Adv. Phys.* **1998**, *47*, 511.
(107) Kodama, R. N.; Makhlouf, S. A.; Berkowitz, A. E. *Phys. Rev. Lett.* **1997**, *79*, 1393.
(108) Speliotis, D. E.; Judge, J. P.; Lynch, W.; Burbage, J.; Keirsted, R. *IEEE Trans. Magn.* **1993**, *29*, 3625.
(109) Kreibig, U.; Vollmer, M. *Optical Properties of Metal Clusters*; Springer: Berlin, 1995.
(110) Maxwell-Garnett, J. C. *Philos. Trans. R. Soc. London* **1904**, *203*, 385.
(111) Bruggemann, D. A. *Ann. Phys. (Leipzig)* **1935**, *24*, 634.
(112) Ung, T.; Liz-Marzán, L. M.; Mulvaney, P. *J. Phys. Chem. B* **2001**, *105*, 3441.
(113) Ung, T.; Liz-Marzán, L. M.; Mulvaney, P. *Colloid Surf. A* **2002**, *202*, 119.
(114) Sönnichsen, C.; Franzl, T.; Wilk, T.; von Plessen, G.; Feldman, J.; Wilson, O.; Mulvaney, P. *Phys. Rev. Lett.* **2002**, *88*, 077402.
(115) Caruso, F.; Caruso, R. A.; Möhwald, H. *Science* **1998**, *282*, 1111.
(116) Caruso, F.; Caruso, R. A.; Möhwald, H. *Chem. Mater.* **1999**, *11*, 3309.
(117) Caruso, F. *Adv. Mater.* **2001**, *13*, 11.
(118) Caruso, F.; Spasova, M.; Salgueiriño-Maceira, V.; Liz-Marzán, L. M. *Adv. Mater.* **2001**, *13*, 1090.
(119) Dokoutchaev, A.; James, J. T.; Koene, S. C.; Pathak, S.; Prakash, G. K. S.; Thompson, M. E. *Chem. Mater.* **1999**, *11*, 2389.
(120) Kobayashi, Y.; Salgueiriño-Maceira, V.; Liz-Marzán, L. M. *Chem. Mater.* **2001**, *13*, 1630.
(121) Schierhorn, M.; Liz-Marzán, L. M. *Nano Lett.* **2002**, *2*, 13.

(122) Oldenburg, S. J.; Averitt, R. D.; Westcott, S. L.; Halas, N. J. *Chem. Phys. Lett.* **1998**, *288*, 243.
(123) Jackson, J. B.; Halas, N. J. *J. Phys. Chem. B* **2001**, *105*, 2743.
(124) Graf, C.; Van Blaaderen, A. *Langmuir* **2002**, *18*, 524.
(125) Salgueiriño-Maceira, V.; Caruso, F.; Liz-Marzán, L. M., submitted to *J. Phys. Chem. B.*
(126) Stamford, J. A.; Justice, J. B. *Anal. Chem.* **1996**, A359.
(127) Smythies, J. *Eur. J. Pharmacol.* **1999**, *1*, 370.
(128) Link, S.; Wang, Z. L.; El-Sayed, M. A. *J. Phys. Chem. B* **1999**, *103*, 3529.
(129) Kobayashi, Y.; Correa-Duarte, M. A.; Liz-Marzán, L. M. *Langmuir* **2001**, *17*, 6375.
(130) Correa-Duarte, M. A.; Kobayashi, Y.; Liz-Marzán, L. M. *J. Nanosci. Nanotechnol.* **2001**, *1*, 95.
(131) Brinker, C. J.; Scherer, G. W. *Sol−Gel Science*, Academic Press: San Diego, CA, 1990.
(132) Selvan, S. T.; Hayakawa, T.; Nogami, M.; Kobayashi, Y.; Liz-Marzán, L. M.; Hamanaka, Y.; Nakamura, A. *J. Phys. Chem. B* **2002**, *106*, 10157.
(133) Hache, F.; Ricard, D.; Flytzanis, C.; Kreibig, U. *Appl. Phys. A* **1988**, *47*, 347.
(134) Joannopoulos, J. D.; Meade, R. D.; Winn, J. N. *Photonic Crystals*; Princeton University Press: Princeton, NJ, 1995.
(135) Jones, J. B.; Sanders, J. V.; Segnit, E. R. *Nature* **1964**, *204*, 990.
(136) For a recent review, see: Imhof, A. In *Nanoscale Materials*; Liz-Marzán, L. M., Kamat, P. V., Eds.; Kluwer Academic Publishers: Boston, 2002.
(137) Norris, D. J.; Vlasov, Y. A. *Adv. Mater.* **2001**, *13*, 371.
(138) Moroz, A. *Europhys. Lett.* **2000**, *50*, 466.
(139) Moroz, A. *Phys. Rev. B* **2002**, *66*, 115109.
(140) Wang, Z. L.; Chan, C. T.; Zhang, W. Y.; Ming, N. B.; Sheng, P. *Phys. Rev. B* **2001**, *64*, 113108.
(141) Míguez, H.; Meseguer, F.; López, C.; Mifsud, A.; Moya, J. S.; Vázquez, L. *Langmuir* **1997**, *13*, 6009.
(142) García-Santamaría, F.; Salgueiriño-Maceira, V.; López, C.; Liz-Marzán, L. M. *Langmuir* **2002**, *18*, 4519.
(143) Nakamura, H.; Mulvaney, P.; Hyde, S. T. *Langmuir*, submitted for publication.
(144) *Adv. Mater.* **2001**, *13* (6) (Special Issue on Photonic Crystals).
(145) Blanco, A.; Chomski, E.; Grabtchak, S.; Ibisate, M.; John, S.; Leonard, S. W.; López, C.; Meseguer, F.; Míguez, H.; Mondia, J. P.; Ozin, G. A.; Toader, O.; van Driel, H. M. *Nature* **2000**, *405*, 437.
(146) Míguez, H.; Chomski, E.; García-Santamaría, F.; Ibisate, M.; John, S.; López, C.; Meseguer, F.; Mondia, J. P.; Ozin, G. A.; Toader, O.; van Driel, H. M. *Adv. Mater.* **2001**, *13*, 1634.
(147) Wang, D.; Salgueiriño-Maceira, V.; Caruso, F.; Liz-Marzán, L. M. *Adv. Mater.* **2002**, *14*, 908.
(148) Rodríguez-González, B.; Salgueiriño-Maceira, V.; García-Santamaría, F.; Liz-Marzán, L. M. *Nano Lett.* **2002**, *2*, 471.
(149) Sader, J.; Larson, I.; Mulvaney, P.; White, L. R. *Rev. Sci. Instrum.* **1995**, *66*, 3789.